LETTERS
PUBLISHED ONLINE: 16 AUGUST 2009 | DOI: 10.1038/NMAT2513
nature materials

Signature of checkerboard fluctuations in the phonon spectra of a possible polaronic metal $La_{1.2}Sr_{1.8}Mn_2O_7$

F. Weber[1,2]*, N. Aliouane[3]*, H. Zheng[4], J. F. Mitchell[4], D. N. Argyriou[3]† and D. Reznik[1,5]†

Charge carriers in low-doped semiconductors may distort the atomic lattice around them and through this interaction form so-called small polarons[1,2]. High carrier concentrations on the other hand can lead to short-range ordered polarons (large polarons)[3,4] and even to a long-range charge and orbital order[5]. These ordered systems should be insulating with a large electrical resistivity[6]. However, recently a polaronic pseudogap was found in a metallic phase of $La_{2-2x}Sr_{1+2x}Mn_2O_7$ (ref. 7). This layered manganite is famous for colossal magnetoresistance associated with a phase transition from this low-temperature metallic phase to a high-temperature insulating phase[7–9]. Broad charge-order peaks due to large polarons in the insulating phase disappear when $La_{2-2x}Sr_{1+2x}Mn_2O_7$ becomes metallic[10]. Investigating how polaronic features survive in the metallic phase, here we report the results of inelastic neutron scattering measurements showing that inside the metallic phase polarons remain as fluctuations that strongly broaden and soften certain phonons near the wavevectors where the charge-order peaks appeared in the insulating phase. Our findings imply that polaronic signatures in metals may generally come from a competing insulating charge-ordered phase. Our findings are highly relevant to cuprate superconductors with both a pseudogap[11,12] and a similar phonon effect associated with a competing stripe order[13].

The competition between a ferromagnetic metallic and paramagnetic insulating phase is behind the famous colossal magnetoresistance (CMR) phenomenon in manganite perovskites such as the quasicubic $La_{1-x}Ca_xMnO_3$ and its bilayer counterpart $La_{2-2x}Sr_{1+2x}Mn_2O_7$. CMR occurs close to a metal–insulator transition temperature, T_c, when applied magnetic field, which favours the ferromagnetic metallic phase, raises T_c. This phase competition appears owing to a natural coupling between magnetism and orbital ordering as Goodenough[14] demonstrated in the 1950s in $LaMnO_3$. In simple terms, the e_g orbitals of Jahn–Teller active Mn^{3+} form a staggered arrangement with the ferromagnetic exchange in MnO_2 layers and antiferromagnetic interplanar coupling. Doping this orbitally ordered Mott insulator with x holes leads to other arrangements where orbital, charge and spin order strongly interact. One such example is the charge and orbitally ordered insulator (known as CE type[15]) at half-doped compositions such as $La_{0.5}Ca_{0.5}MnO_3$ (ref. 16) or $LaSr_2Mn_2O_7$ (refs 17–19) where the e_g charge is localized on alternate Mn sites producing to first-order distinct Mn^{3+} and Mn^{4+} sites[16,18] (see Fig. 1b). (Measured charge separation between nominal Mn^{3+} and Mn^{4+} ions is found to be of the order of 0.2–0.4e for half-doped manganites[16,18].) The Jahn–Teller effect and orbital ordering of the e_g charge induces a characteristic distortion with a superlattice peak at a wavevector of $\mathbf{q}_{CE} = (1/4, -1/4, 0)$ in $LaSr_2Mn_2O_7$. For intermediate compositions, the frustration of the charge and orbital ordering results in a ferromagnetic metallic ground state, with CMR in the vicinity of T_c (ref. 5). A phase transition to an insulating phase occurs at

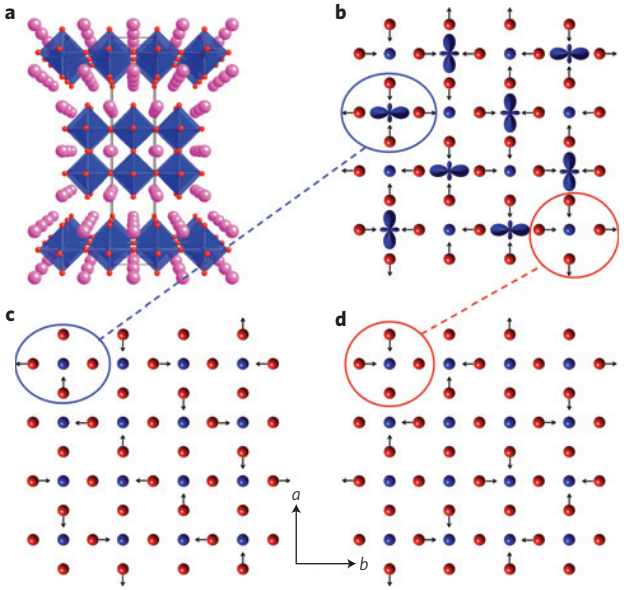

Figure 1 | Correspondence between CE order and phonon vibration patterns. a, Layered crystal structure of $La_{2-2x}Sr_{1+2x}Mn_2O_7$ with La (purple) atoms between the MnO_6 octahedra (Mn: blue, O: red). **b**, Schematic diagram of the displacements of oxygens from the ideal unordered structure in long-range CE-ordered half-doped compositions ($x = 0.5$). The drawn e_g orbitals indicate the Mn^{3+} ions. Mn displacements are not shown. **c**,**d**, Eigenvectors of the transverse (**c**) and longitudinal (**d**) bond-stretching phonons with $\mathbf{q} = (0.25, 0.25, 0)$. Small Mn displacements are not shown. Short-range CE fluctuations should couple strongly to both the longitudinal and transverse phonons. The dashed lines indicate the partial matching of oxygen displacements of the CE order and of the phonon eigenvectors.

[1]Forschungszentrum Karlsruhe, Institut für Festkörperphysik, POB 3640, D-76021 Karlsruhe, Germany, [2]Physikalisches Institut, Universität Karlsruhe, D-76128 Karlsruhe, Germany, [3]Helmholtz-Zentrum Berlin für Materialen und Energy, Glienicker Str. 100, D-14109 Berlin, Germany, [4]Materials Science Division, Argonne National Laboratory, Argonne, Illinois, 60439, USA, [5]Laboratoire Léon Brillouin, CEA Saclay, F-91191 Gif-sur-Yvette, France. *Present addresses: Materials Science Division, Argonne National Laboratory, Argonne, Illinois, 60439, USA (F.W.); Institute For Energy Technology, PO Box 40, NO-2027 Kjeller, Norway (N.A.). †e-mail: argyriou@helmholtz-berlin.de; dmitri.reznik@cea.fr.

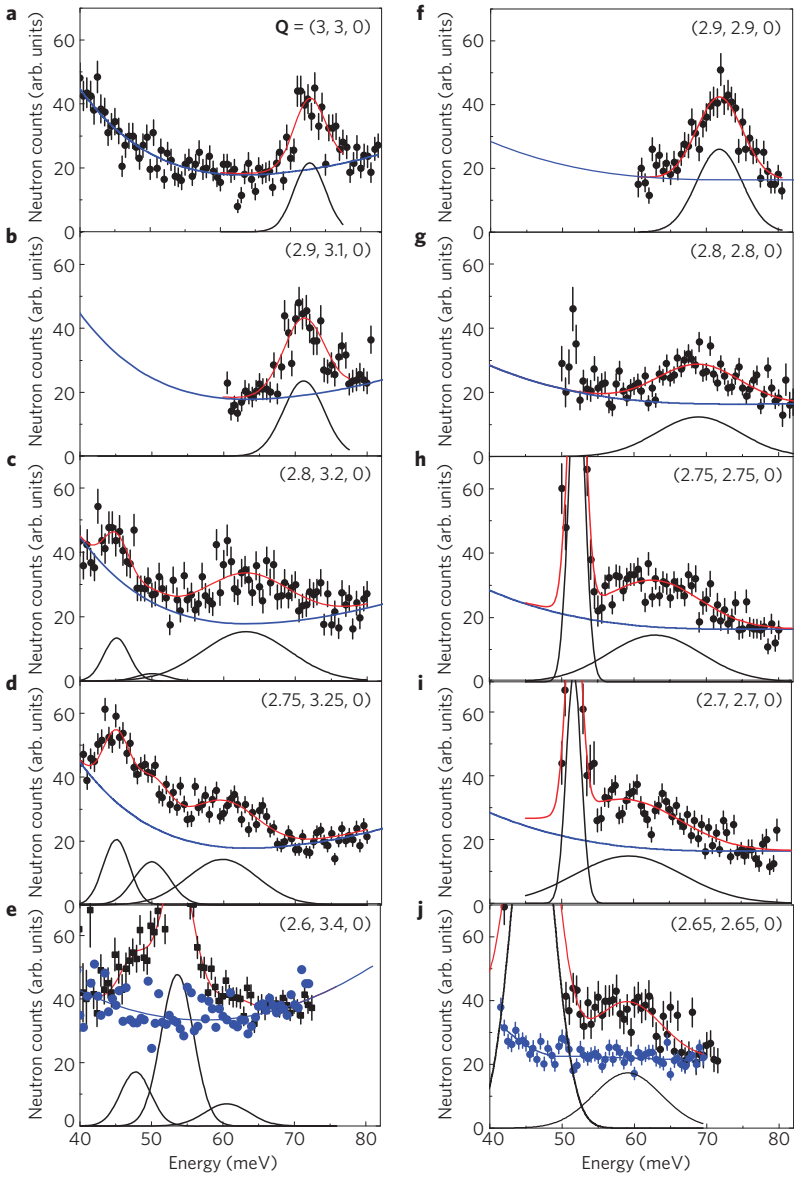

Figure 2 | Representative constant-Q scans for transverse and longitudinal phonons dispersing in the (1, 1, 0) direction. The data are normalized to a monitor of 50,000 neutron counts, which corresponds to a counting time of 5 min for an energy transfer $E = 70$ meV. The scans shown in **e** and **j** are each measured in different runs and therefore have different backgrounds. See Supplementary Information for details about the background determination. The scan at $\mathbf{Q} = (2.6, 3.4, 0)$ was measured with a final energy $E_f = 30.5$ meV. All other data were measured with $E_f = 35$ meV. Functions fitted to the background data are shown as blue lines. The black lines are Gaussians fitted to the data after background subtraction. The red lines represent the background function plus the Gaussian fits. The data were taken at $T = 10$ K. The error bars represent s.d.

elevated temperatures where 15-Å clusters of CE order[3] mingle with charge-delocalized clusters[20] as clearly visible diffuse elastic or quasielastic diffraction peaks in the vicinity of $\mathbf{q}_{CE}$ (ref. 3). (It is important to note that diffuse scattering from lattice polarons represents the correlated atomic displacements due to charge localization and is different from the scattering that arises from single polarons (uncorrelated single charges)[21].) Below T_c, ferromagnetic fluctuations quickly melt the local CE correlations[3,18]. Instability of these polarons in the presence of ferromagnetism and applied magnetic field leads to CMR close to T_c. This ferromagnetic metal has poor conductivity and a small carrier scattering length[9].

Whereas the disappearance of the polaronic scattering below T_c was thought to mark the onset of a conventional double-exchange metallic ground state, recent photoemission measurements of the bilayer manganite $La_{2-2x}Sr_{1+2x}Mn_2O_7$ with $x = 0.4$ (ref. 7) show an unconventional pseudogap in many respects similar to features predicted to arise from single polarons[22,23]. These results seem to imply a coexistence between polarons and metallic electrical resistivity, which defines a polaronic metal. Its nature remains enigmatic. We present results of inelastic neutron scattering measurements suggesting that polaronic effects in the bilayer manganites are dominated by strong fluctuations that mimic the extended lattice distortions of the CE type that emerge above T_c. Their experimental signature is phonon broadening and softening at the wavevectors where diffuse scattering due to short-range CE order appears above T_c. Our findings show that the polaronic degrees of freedom dominate the properties of the ferromagnetic metallic phase of this CMR manganite and reveal that in the strong coupling limit a polaronic metal is a viable ground state.

We focused on the Mn–O bond-stretching phonon branches dispersing in the [110] direction in the bilayer CMR compound,

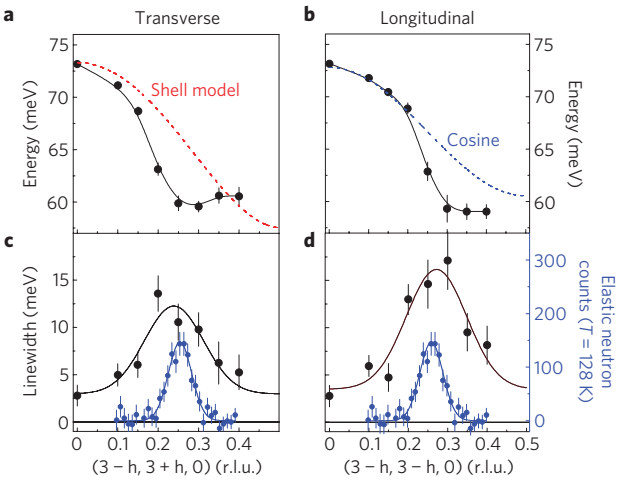

Figure 3 | Dispersions and linewidths of transverse and longitudinal bond-stretching phonons in the (1, 1, 0) direction of $La_{1.2}Sr_{1.8}Mn_2O_7$. **a**,**b**, The data points represent measured phonon energies; the black lines are guides to the eye; the red dashed line in **a** is the dispersion calculated by the shell model. **c**,**d**, The black circles are phonon full-width at half-maximum after correction for the experimental resolution. The black lines are guides to the eye. The blue circles represent the elastic intensity (right-hand scale) of the short-range charge and orbital order above $T_c = 115$ K. The error bars represent s.d.

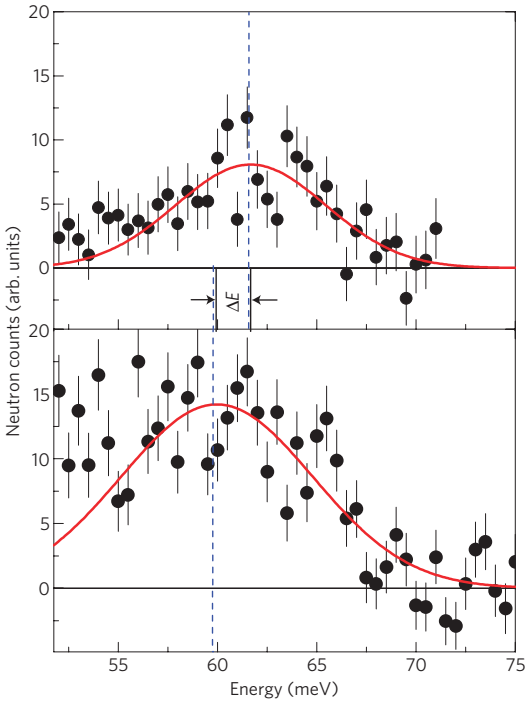

Figure 4 | Background-subtracted phonon spectra at Q = (2.75, 3.25, 0). The background was measured separately at the two temperatures: 150 K (top) and 10 K (bottom). The red lines are Gaussians fitted to the observed peaks for $E > 56$ meV (see text). The vertical dashed lines mark the fitted frequencies of the bond-stretching phonon at $T = 10$ and 150 K.

$La_{1.2}Sr_{1.8}Mn_2O_7$. MnO_6 octahedra in this manganite align along the three crystallographic axes (Fig. 1a). Lattice distortions in the CE polaronic state have the ordering wavevector $\mathbf{q}_{CE} = (1/4, -1/4, 0)$ (Fig. 1b). The lattice deformation around the nominal Mn^{3+} site (indicated by the occupied e_g orbital) corresponds to a part of the eigenvector of the transverse phonon (Fig. 1c), whereas the deformation around the nominal Mn^{4+} site corresponds to a part of the eigenvector of the longitudinal one (Fig. 1d). This partial matching provides a natural mechanism of strong coupling between fluctuating CE distortions and both the transverse and the longitudinal phonons at the same wavevector.

In contrast, in the commonly studied '113' quasicubic compounds such as $La_{0.7}Sr_{0.3}MnO_3$, tilted octahedra result in extra bond-bending branches folded in from different parts of the Brillouin zone. These mix with the stretching vibrations away from the zone centre[24,25], prohibiting the study of pure bond-stretching modes. Previous studies of quasicubic manganites have not been able to link very strong temperature-induced changes in phonon intensities[26,27] with specific charge or orbital fluctuations. Thus, the bilayer manganites are ideal for investigating dispersions of bond-stretching modes.

Our sample was a high-quality 0.5 cm^3 single crystal of $La_{1.2}Sr_{1.8}Mn_2O_7$ with the ferromagnetic metallic transition temperature measured at 115 K. The experiments were carried out on the 1 T triple-axis spectrometer at the ORPHEE reactor, using doubly focusing Cu220 monochromator and PG002 analyser crystals. The final energies were fixed at 30.5 meV or 35 meV. The components $(Q_x, Q_y, 0)$ are expressed in reciprocal lattice units (r.l.u.) (1 r.l.u. $= 2\pi/a$, $a = 3.88$ Å). Measurements were carried out in the constant-momentum-transfer $\mathbf{Q}$ mode, $\mathbf{Q} = \boldsymbol{\tau} + \mathbf{q}$, and $\boldsymbol{\tau}$ is a reciprocal lattice point. The longitudinal/transverse branch was measured at $\mathbf{q} = (-h, -h, 0)/(-h, +h, 0)$ $(0 \leq h \leq 0.5)$ respectively.

Small bond-stretching phonon structure factors were overcome by careful selection of the experimental conditions, coverage of two Brillouin zones and very long counting times of as much as 1 h per point at 10 K and 2 h at 150 K. We assigned the observed phonon peaks by comparing our results both to shell model predictions and to the previous measurements of layered cuprate perovskites, $La_{2-x}Sr_xCuO_4$ (ref. 28). The shell model has been developed for the cuprates and has already been successfully applied to a cubic manganite[24]. It predicts phonon dispersions reasonably well with the notable exception of the longitudinal bond-stretching branch. This is also true for the bilayer manganites. Further special force constants can adjust calculated dispersions of the stretching branches to agree with the measured ones. After the adjustment, the model makes good qualitative predictions of phonon eigenvectors, and, therefore, intensities, which we had used to identify bond-bending and bond-stretching peaks (Fig. 2). The peak assignment procedure and background determination are described in detail in the Supplementary Information. The resolution function was calculated for our experimental set-up and folded with the dispersions of the bond-stretching branches to obtain the intrinsic phonon linewidths shown in Fig. 3c,d.

Figure 2 shows representative scans between 40 and 80 meV measured deep inside the ferromagnetic metallic phase (at 10 K) in the Brillouin zone adjacent to $\boldsymbol{\tau} = (3, 3, 0)$. The zone-centre bond-stretching vibration at $\mathbf{Q} = (3, 3, 0)$ is at 73 meV (Fig. 2a). There is no peak corresponding to the 43 meV bond-bending vibration in Fig. 2a because its structure factor is zero. We measured its dispersion around $\mathbf{Q} = (4, 4, 0)$ where its structure factor is strong. Another bond-bending peak, at 33 meV, is just below the energy range of Fig. 2a (see Supplementary Information for details).

The transverse bond-stretching branch direction disperses steeply downwards along $(h, -h, 0)$ and the transverse bending branches disperse gradually upwards. They do not overlap until $h = 0.4$, enabling a study of pure bond-stretching modes at $(0 \leq h \leq 0.35)$. They can be traced as a high-energy shoulder of the much stronger bending modes further towards the zone boundary $(h = 0.5)$.

The longitudinal bond-stretching branch disperses downwards along $(h, h, 0)$, whereas the higher-energy bending mode disperses sharply upwards with an anticrossing near $h = 0.3$. However, the

structure factor for this bending mode remains near zero in the $\mathbf{Q} = (3, 3, 0)$ Brillouin zone up to close to the zone boundary ($h = 0.5$); thus, the observed intensity unambiguously comes from the stretching mode at ($0 \leq h \leq 0.4$) (see Supplementary Information for details).

Both the transverse and longitudinal stretching branches dip sharply and have a linewidth maximum (shortest lifetime) near $\mathbf{q}_{CE}$ (Fig. 3), which indicates strong electron–phonon coupling deep in the metallic state. In $La_{1.2}Sr_{1.8}Mn_2O_7$, $\mathbf{q}_{CE}$ corresponds to the maximum of the diffuse scattering at 128 K (Fig. 3c,d) due to static (frozen) short-range CE order[18]. This observation highlights the close relationship between the polaronic insulating phase and the phonon renormalization in the metallic phase. The $\mathbf{q}$-width of the phonon broadening is larger than that of the elastic peak. It corresponds to a correlation length of 2–3 unit cells compared with 4 unit cells in the insulating phase.

This phonon anomaly is absent from the equivalent branches in the cuprates[28]. It also seems to be absent from the quasicubic $La_{0.7}Sr_{0.3}MnO_3$ where the downward dispersion of the transverse branch was reported to continue to lower energies at low temperatures[24]. This difference may be explained by the fact that CE order does not appear in this system in the paramagnetic state and that the continual softening towards the zone boundary may result from interaction with uncorrelated small polarons.

The longitudinal branch disperses downwards (Fig. 3b), whereas the shell model suggests an upward dispersion. This discrepancy is similar to overdoped $La_{1.7}Sr_{0.3}CuO_4$ and the overall downward dispersion most probably reflects metallic behaviour as opposed to an exotic effect[28]. Where the difference between $La_{1.2}Sr_{1.8}Mn_2O_7$ and the cuprates is pronounced, is near $\mathbf{q}_{CE}$: in the former there is a sharp dispersion dip, accompanied by linewidth broadening, whereas in the latter it follows a cosine dispersion with a roughly constant linewidth.

We now discuss what happens above T_c when the static short-range CE order appears. Much longer counting times are required here because static distortions suppress coherent phonon intensities by almost a factor of 2 and the background increases by a factor of 1.5. For this reason, we measured only one wavevector at $\mathbf{Q} = (2.75, 3.25, 0)$ at 150 K, well above the static polaron-ordering temperature.

Figure 4 shows the background-subtracted phonon spectra at $\mathbf{Q} = (2.75, 3.25, 0)$ measured at 10 and 150 K. As the contribution of the lower-energy phonons cannot be satisfactorily evaluated, we fitted the data with a single Gaussian above 56 meV. In this energy range, the observed intensity is of pure bond-stretching character (as follows from Fig. 2d). We see no indication of anharmonic broadening and softening usually expected at increased temperatures as the amplitude of atomic motion increases.

Broadening due to static disorder is expected to increase above T_c owing to the formation of CE polarons. As such an increase does not occur for the bond-stretching phonons, their broadening and softening at low temperatures must be of electronic origin. We note that this behaviour is in contrast with the bond-bending phonon at 43 meV, which does broaden above T_c (see Supplementary Fig. S3). The question, whether the temperature dependence in Fig. 4 originates from the increased availability of electronic states in the low-temperature phase or from the enhanced charge-phonon coupling, cannot be answered at this point.

We conclude that phonon renormalization in the [110] direction is dominated by a fluctuation of CE type, which we assign to CE dynamic polarons. This fluctuation exists below T_c and then condenses into the static or quasistatic order[18] at the metal–insulator transition. This novel phenomenon is unusual, because polaron fluctuations have been observed at $T < 0.1\,T_c$ and therefore do not appear to be associated with the critical behaviour near the phase transition. The polaron fluctuation around $\mathbf{q}_{CE} = (1/4, -1/4, 0)$ may be related to the strong nesting of the Fermi surface[1] near the same wavevector[7,8]. More work is necessary to clarify the association between these two phenomena.

Our measurements offer the defining characteristics of a polaronic metal[7]. It combines quasiparticles that exist over a small portion of the Fermi surface with CE-type modes inherited from the polaronic insulator above T_c, which strongly renormalize certain phonons. Furthermore, charge transport below T_c is dominated by coherent polarons with overlapping wavefunctions, in contrast to the classical single polarons found at small carrier concentrations. Indeed, above T_c such overlap leads to static local CE order. One cannot avoid the striking similarities between the [110] direction in this manganite and the [100] direction in the superconducting cuprates where charge fluctuations in the form of stripes seem to induce a similar phonon renormalization. It is intriguing that real and imaginary parts of the low-temperature phonon self-energies in the cuprates at $\mathbf{q} \approx (1/4, 0, 0)$ and in the manganites at $\mathbf{q} \approx (1/4, 1/4, 0)$ are very close. This similarity indicates that dynamic charge stripes in the cuprates are somehow analogous to the fluctuating checkerboard-like CE polarons in the manganites. Exploring this connection will no doubt shed light on many unresolved questions for both classes of compounds where pseudogap-like phases have a critical role.

Received 5 August 2008; accepted 15 July 2009; published online 16 August 2009

References

1. Holstein, T. Studies of polaron motion. Part II. The small polaron. *Ann. Phys.* **8,** 343–389 (1959).
2. Emin, D. Existence of free and self trapped carriers in insulators. *Adv. Phys.* **22,** 57–116 (1973).
3. Adams, C. P., Lynn, J. W., Mukovskii, Y. M., Arsenov, A. A. & Shulyatev, D. A. Charge ordering and polaron formation in the magnetoresistive oxide $La_{0.7}Ca_{0.3}MnO_3$. *Phys. Rev. Lett.* **85,** 3954–3957 (2000).
4. Dai, P. *et al.* Short-range polaron correlations in the ferromagnetic $La_{1-x}Ca_xMnO_3$. *Phys. Rev. Lett.* **85,** 2553–2556 (2000).
5. Dagotto, E. Complexity in strongly correlated electronic systems. *Science* **309,** 257–262 (2005).
6. Millis, A., Littlewood, P. & Shraiman, B. Double exchange alone does not explain the resistivity of $La_{1-x}Sr_xMnO_3$. *Phys. Rev. Lett.* **74,** 5144–5147 (1995).
7. Manella, N. *et al.* Nodal quasiparticles in pseudogapped colossal magnetoresistive manganites. *Nature* **438,** 474–478 (2005).
8. Dessau, D. S. *et al.* **k**-dependent electronic structure, a large 'ghost' Fermi surface, and a pseudogap in a layered magnetoresistive oxide. *Phys. Rev. Lett.* **81,** 192–195 (1998).
9. Chuang, Y.-D. *et al.* Fermi surface nesting and nanoscale fluctuating charge/orbital ordering in colossal magnetoresistive oxides. *Science* **292,** 1509–1513 (2001).
10. Argyriou, D. N. *et al.* Glass transition in the polaron dynamics of colossal magnetoresisitive manganites. *Phys. Rev. Lett.* **89**036401 (2002).
11. King, D. M. *et al.* Electronic structure evolution from Mott insulator to superconductor—an angle-resolved photoemission investigation. *J. Phys. Chem. Solids* **56,** 1865–1869 (1995).
12. Damascelli, A., Hussain, Z. & Shen, Z.-X. Angle-resolved photoemission studies of the cuprate superconductors. *Rev. Mod. Phys.* **75,** 473–541 (2003).
13. Reznik, D. *et al.* Electron–phonon coupling reflecting dynamic charge inhomogeneity in copper oxide superconductors. *Nature* **440,** 1170–1173 (2006).
14. Goodenough, J. B. Theory of the role of covalence in the perovskite-type manganites $La_{1-x}M(II)_xMnO_3$. *Phys. Rev.* **100,** 564–573 (1955).
15. Wollan, E. O. & Koehler, W. C. Neutron diffraction study of the magnetic properties of the series of perovskite-type compounds $La_{1-x}Ca_xMnO_3$. *Phys. Rev.* **100,** 545–563 (1955).
16. Radaelli, P. G., Cox, D. E., Marezio, M. & Cheong, S. Charge, orbital, and magnetic ordering in $La_{0.5}Ca_{0.5}MnO_3$. *Phys. Rev. B* **55,** 3015–3023 (1997).
17. Li, J. Q., Matsui, Y., Kimura, T. & Tokura, Y. Structural properties and charge-ordering transition in $LaSr_2Mn_2O_7$. *Phys. Rev. B* **57,** R3205–R3208 (1998).
18. Argyriou, D. N. *et al.* Charge ordering and phase competition in the layered perovskite $LaSr_2Mn_2O_7$. *Phys. Rev. B* **61,** 15269–15276 (2000).

19. Li, Q. *et al.* Reentrant orbital order and the true ground state of $LaSr_2Mn_2O_7$. *Phys. Rev. Lett.* **98,** 167201 (2007).
20. Sun, Z. *et al.* A local metallic state in globally insulating $La_{1.24}Sr_{1.76}Mn_2O_7$ well above the metal–insulator transition. *Nature Phys.* **3,** 248–252 (2007).
21. Vasiliu-Doloc, L. *et al.* Charge melting and polaron collapse in $La_{1.2}Sr_{1.8}Mn_2O_7$. *Phys. Rev. Lett.* **83,** 4393–4396 (1999).
22. Rosch, O. & Gunnarsson, O. Dispersion of incoherent spectral features in systems with strong electron–phonon coupling. *Eur. Phys. J. B* **43,** 11–18 (2005).
23. Mishchenko, A. S. & Nagaosa, N. Electron–phonon coupling and a polaron in the t–J model: From the weak to the strong coupling regime. *Phys. Rev. Lett.* **93,** 036402 (2004).
24. Reichardt, W. & Braden, M. Anomalous features in the bond stretching vibrations of $La_{1-x}Sr_xMnO_3$. *Physica B* **263–264,** 416–420 (1999).
25. Reznik, D. & Reichardt, W. Bond-bending and bond-stretching phonons in ferromagnetic $La_{1-x}Sr_xMnO_3$. *Phys. Rev. B* **71,** 092301 (2005).
26. Zhang, J. *et al.* Jahn–Teller phonon anomaly and dynamic phase fluctuations in $La_{0.7}Ca_{0.3}MnO_3$. *Phys. Rev. Lett.* **86,** 3823–3826 (2001).
27. Reznik, D. & Reichardt, W. Phonon mechanism of the ferromagnetic transition in $La_{1-x}Sr_xMnO_3$. Preprint at <http://arxiv.org/abs/cond-mat/0312368> (2003).
28. Pintschovius, L., Reznik, D. & Yamada, K. Oxygen phonon branches in overdoped $La_{1.7}Sr_{0.3}CuO_4$. *Phys. Rev. B* **74,** 174514 (2006).

Acknowledgements

The authors would like to thank M. Braden and L. Pintschovius for helpful discussions and suggestions, and M. Braden and W. Reichardt for allowing us to use shell model parameters for $La_{2-2x}Sr_{1+2x}Mn_2O_7$ that they found in a separate investigation. D.N.A. and D.R. thank Dan Dessau and Jan Zaanen for discussions. Work at Argonne National Laboratory was supported under Contract No. DE-AC02-06CH11357 by UChicago Argonne, LLC, Operator of Argonne National Laboratory, a US Department of Energy Office of Science Laboratory. N.A, was supported in part by the Hytrain Project of the Marie Curie Research Training Network funded under the EC's 6th Framework Human Resources and Mobility Program.

Author contributions

D.R. and D.N.A. conceived and oversaw the project. H.Z. and J.F.M. grew the single-crystal sample. The first measurements were carried out by F.W., N.A., D.N.A. and D.R. F.W. and D.R. carried out many further measurements. F.W. carried out the data analysis and lattice dynamics calculations. D.R. and D.N.A. wrote the manuscript with revisions from F.W. F.W. and D.R. prepared figures and Supplementary Information.

Additional information

Supplementary information accompanies this paper on www.nature.com/naturematerials. Reprints and permissions information is available online at http://npg.nature.com/reprintsandpermissions. Correspondence and requests for materials should be addressed to D.N.A. or D.R.